Journal of Electronic Materials (2025) 54:11053–11068
https://doi.org/10.1007/s11664-025-12380-x

ORIGINAL RESEARCH ARTICLE

Enhancement of Ionic Conduction in Alginate–PVA Polymer Electrolytes Doped with Ammonium Thiocyanate

N. A. Wahab[1] · M. A. Saadiah[2] · N. F. Mazuki[1] · N. M. Ghazali[1] · K. Aoki[3] · Y. Nagao[3] · A. S. Samsudin[1,4]

Received: 3 September 2024 / Accepted: 25 August 2025 / Published online: 23 September 2025

Abstract

This study explores the eco-friendly enhancement of ionic conduction properties and transport properties in solid polymer electrolytes (SPEs) based on a sustainable alginate (Al) and polyvinyl alcohol (PVA) blend, modified by varying weight percentages (wt%) of ammonium thiocyanate (NH_4SCN) using a solution casting technique. The SPE system was characterized using Fourier-transform infrared (FTIR) spectroscopy, Thermal gravimetric analysis (TGA), X-ray diffraction (XRD), scanning electron microscopy (SEM), and electrical impedance spectroscopy (EIS). SEM images revealed significant modifications in surface morphology correlating with different NH_4SCN contents. FTIR analysis confirmed interactions between the alginate–PVA matrix and NH_4SCN, evidenced by shifts and changes in peak intensities resulting from the protonation of H^+-OOC. Impedance studies indicated a reduction in bulk resistance (R_b) with increasing NH_4SCN content up to 35 wt%, achieving the highest ionic conductivity of 3.4×10^{-4} S cm^{-1} at room temperature. Temperature dependence studies revealed that the SPE systems adhere to Arrhenius behavior, with regression values nearing unity. Additionally, dielectric response analysis showed a consistent trend with ionic conductivity, indicating enhanced transport properties. These findings highlight the potential of alginate–PVA–NH_4SCN SPEs for use in environmentally friendly applications such as proton batteries and supercapacitors, offering a sustainable alternative in energy storage solutions.

Keywords Ionic conductivity · Transport properties · Intermolecular interaction · Grotthuss mechanism

Introduction

The increasing demand for advanced electrochemical devices, such as supercapacitors, fuel cells, and sensors, is driving research towards more eco-friendly and efficient solutions. These devices are essential for energy storage and conversion, which are pivotal for a sustainable energy future. Extensive research has explored various materials as electrolytes in these applications, leading to significant advancements. One such advancement is the development of solid polymer electrolytes (SPEs), which address the flammability and leakage issues associated with conventional liquid electrolytes. SPEs offer several advantages, including ease of fabrication, low-cost processing, and good shelf life. Moreover, SPEs often incorporate natural polymers that are biodegradable and non-hazardous, making them more environmentally friendly compared to synthetic polymers [1, 2].

Various polymers, such as polyvinyl alcohol (PVA) [3], chitosan [4], methylcellulose [5], and pene oxide [6], have been investigated for the development of polymer electrolytes. PVA is particularly favored due to its low cost, hydrophilicity, suitable mechanical properties, and biocompatibility. Its exceptional chemical stability, physicochemical attributes, high dielectric constant, efficient charge storage capacity, and dopant-dependent electrical and optical properties make it widely used in several industrial sectors [2]. However, the primary challenge in developing these promising electrolytes is achieving high ionic conductivity at room

✉ A. S. Samsudin
ahmadsalihin@umpsa.edu.my

1 Ionic Materials Team, Faculty of Industrial Sciences & Technology, University Malaysia Pahang Al-Sultan Abdullah, 26300 Kuantan, Pahang, Malaysia

2 Department of Chemistry, Centre for Foundation Studies, International Islamic University Malaysia, 26300 Gambang, Pahang, Malaysia

3 School of Materials Science, Japan Institute of Science and Technology, Asahidai, Nomi City, Ishikawa, Japan

4 Centre for Automotive Engineering, Universiti Malaysia Pahang Al-Sultan Abdullah, 26600 Pekan, Pahang, Malaysia

temperature, which is essential for the efficient operation of electrochemical devices [7].

Alginate, a naturally occurring polymer derived from brown seaweed, has demonstrated compatibility with a wide range of chemicals, leading to higher conductivity values in various composites. Significant increases in ionic conductivity have been observed in chitosan–sodium alginate (4.2×10^{-2} S cm^{-1}) [8], alginate–graphene oxide (13.2×10^{-3} S cm^{-1}) [9], alginate–alumina (25.6×10^{-3} S cm^{-1}) [10], and alginate–titanium dioxide (17.3×10^{-3} S cm^{-1}) [11] composites. These examples highlight the potential of alginate-based composites to achieve desirable electrochemical characteristics. Blending two polymers to serve as hosts is an effective way to enhance the conductivity of electrolytes. For instance, the conductivity value of an alginate–PVA biopolymer mix system, as reported by Ghazali et al., was 7.52×10^{-8} S cm^{-1}, which is slightly less than the conductivity of pure PVA and alginate (~ 10^{-7} to 10^{-6} S cm^{-1}) [8]. However, Saadiah et al. found that combining two polymers increased the number of complexation sites, thereby improving ion mobility and polymer chain flexibility [8]. Adding an ionic salt to the mixture further enhances the conducting properties.

In this context, the strategic doping of alginate–PVA polymer electrolytes with ammonium thiocyanate (NH_4SCN) presents a promising approach to enhance ionic conduction while maintaining the environmental benefits of the polymer blend. NH_4SCN is chosen for its ability to facilitate ion transport, potentially improving the overall performance of the SPE. By investigating structural interactions through Fourier-transform infrared (FTIR) spectroscopy, thermal gravimetric analysis (TGA), X-ray diffraction (XRD), surface morphology via scanning electron microscopy (SEM), and impedance spectroscopy (EIS), this study provides a comprehensive analysis of the modified SPEs. This research presents the synthesis and characterization of alginate–PVA-based SPEs doped with varying concentrations of NH_4SCN. It aims to understand how the incorporation of NH_4SCN influences the ionic conductivity and other electrochemical properties of the SPEs, revealing the effect of dissolving salt in the polymer host and providing charge carriers to the electrolyte.

These insights not only contribute to the fundamental understanding of polymer electrolyte systems but also pave the way for the development of sustainable energy storage solutions. By optimizing the composition and properties of SPEs, this study aims to address the challenges of current energy storage technologies, providing a viable alternative that aligns with environmental sustainability goals.

Experimental

Sample Preparation

The SPE system, comprising alginate–PVA polymer blends as the host polymer and NH_4SCN as the ionic dopant, was prepared using the solution-casting technique. Amounts of 0.60 g pure PVA (Merck Schuchardt, average molecular weight of 70,000 g/mol, 85% hydrolyzed) and 1.40 g sodium alginate (Sigma Aldrich, average molecular weight 216.12 g/mol) were dissolved in distilled water under constant magnetic stirring in the range of 400–500 rpm at room temperature until a homogeneous solution was obtained. All the chemicals were used as received without further purification. Varying weight percentages of NH_4SCN (Sigma Aldrich, molecular weight of 76.12 g/mol) from 5 to 45 wt% were added to the solution with continuous stirring at the same speed until fully dissolved. The mixture was then cast into Petri dishes and dried at 50–60 ℃ in a vacuum oven until a solid film formed completely. The appearance of the sample and its designation are shown in Fig. 1 and Table I, respectively.

Sample Characterization

Fourier-Transform Infrared (FTIR) Spectroscopy

The prepared Al–PVA–NH_4SCN SPEs were characterized using FTIR spectroscopy (PerkinElmer) over a wavenumber range of 700–4000 cm^{-1} with an attenuated total reflection (ATR) accessory. Ten scans at 2 cm^{-1} resolution were used to acquire the ATR-FTIR spectra.

Thermal Gravimetric Analysis–Differential Scanning Calorimetry (TGA-DSC)

The thermal stability of the SPEs was analyzed using a Mettler Toledo TGA-DSC. Approximately 2 mg of each sample was placed in a silica crucible and heated from 30 to 800 °C at a rate of 10 °C/min under a nitrogen atmosphere with a flow rate of 20 mL/min.

X-ray Diffraction (XRD)

XRD analysis was conducted using a Rigaku MiniFlex II equipped with a nickel-filtered Cu Kα ($\lambda = 0.154$ nm) tube operated at 30 kV and 15 mA. The XRD profiles of the Al–PVA–NH_4SCN samples were recorded over a 2θ range from 5° to 80° at ambient temperature.

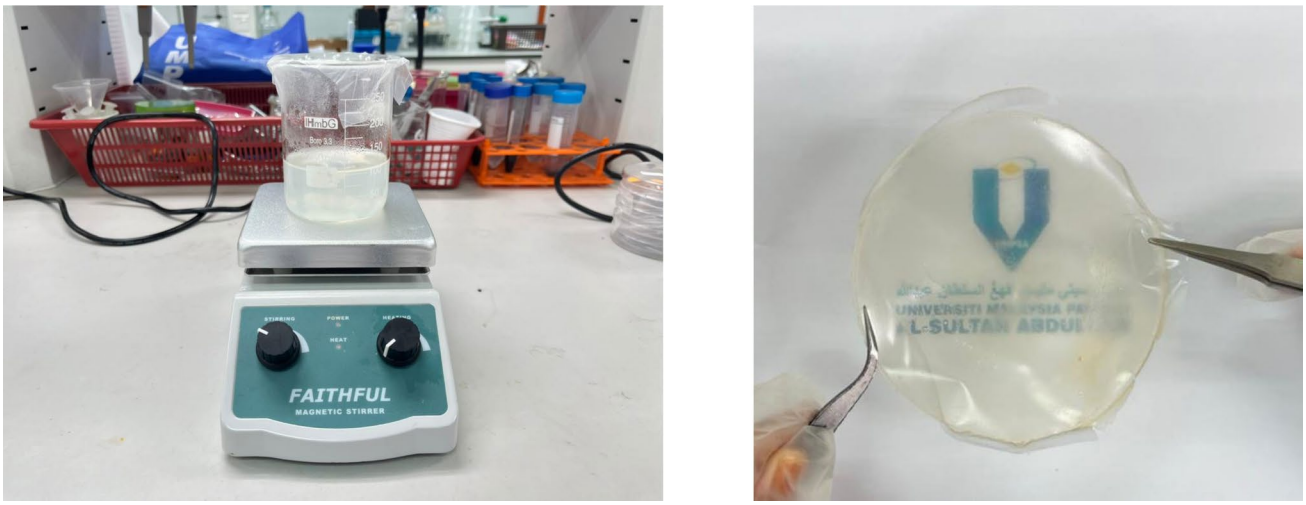

Fig. 1 Sample preparation and the outcome sample of Al–PVA–NH_4SCN.

Table I Composition of Al–PVA–NH_4SCN

Sample designation	NH_4SCN (wt%)	NH_4SCN (g)
APN1	5	0.1052
APN2	10	0.2222
APN3	15	0.3529
APN4	20	0.5000
APN5	25	0.6667
APN6	30	0.8571
APN7	35	1.0769
APN8	40	1.3333
APN9	45	1.6363

Scanning Electron Microscopy (SEM)

The surface morphology of the Al–PVA–NH_4SCN samples was examined using a Tabletop Miniscope TM3030Plus (Hitachi High Technologies, Japan) equipped with an energy-dispersive X-ray spectrometer (EDX). The samples were observed at a magnification of ×400 and analyzed at accelerating voltages of 10 kV and 15 kV.

Electrical Impedance Spectroscopy (EIS)

The conduction properties of the Al–PVA–NH_4SCN SPE samples were assessed using EIS. Small discs (2 cm in diameter) were cut from the samples and sandwiched between two stainless steel electrodes. The EIS measurements were conducted using a HIOKI 3532-50 LCR Hi-Tester over a frequency range of 50–1 MHz and temperatures ranging from 30 °C to 80 °C. The conductivity (σ) was calculated using:

$$\sigma = \frac{t}{R_b A} \tag{1}$$

where t is the thickness of the film, A is contact surface area, and R_b is represented as bulk resistance.

The dielectric constant, ε_r for the Al–PVA–NH_4SCN SPE system was defined by:

$$\boldsymbol{\varepsilon_r} = \frac{\boldsymbol{Z_i}}{\boldsymbol{Z^2}_r + \boldsymbol{Z^2}_i}\left(\frac{\boldsymbol{d}}{\boldsymbol{\omega \varepsilon_\circ A}}\right) \tag{2}$$

where Z_r and Z_I are the real and imaginary parts of complex permittivity, respectively, d is half the thickness of the polymer electrolyte, ω is equal to $2\pi fA$ or the angular frequency corresponding to the minimum in the imaginary impedance, f is the frequency in Hz, ε_o is the permittivity of free space (8.85×10^{-14} F cm^{-1}), and A is the electrolyte–electrode contact area.

Transport properties (D, μ, and n) of the Al–PVA–NH_4SCN system were determined by:

$$\boldsymbol{D} = \frac{(\boldsymbol{k_2 \varepsilon_r \varepsilon_\circ A})^2}{\boldsymbol{T_2}} \tag{3}$$

$$\boldsymbol{\mu} = \frac{\boldsymbol{e(k_2 \varepsilon_r \varepsilon_\circ A)^2}}{\boldsymbol{k_b T t_2}} \tag{4}$$

The number density of charge carriers (η) can be obtained using:

$$\eta = \frac{\sigma k_2 T t_2}{\left(e k_b \varepsilon_r \varepsilon_\circ A\right)^2} \tag{5}$$

where D is the difference coefficient, k_2 is the capacitance of the constant phase element (CPE) caused by the electrical double layer formed at the electrode–electrolyte interface during the impedance measurement, ε_o is the vacuum permittivity, A is the electrode–electrolyte contact area, and τ_2 is a time constant corresponding to the maximum dissipative loss curve, equal to $1/\omega_2$.

K_2 in Eq (3)-(5) were calculated using:

$$K_2 = \frac{\lambda_D}{\varepsilon_r \varepsilon_o A} \tag{6}$$

where λ_D is the Debye length and calculated using:

$$\lambda_D = \sqrt{\frac{\varepsilon_r \varepsilon_o k_b T}{Z^2 e^2 n}} \tag{7}$$

Transference Number

DC polarization techniques were used to investigate the relationship between the ion diffusion and the conductivity behavior of the Al–PVA–NH_4SCN solid polymer electrolytes. The optimal sample was to analyze the H+ transference number using an impedance analyzer (PGSTAT M101 with FRA32M module, Autolab) and a DC voltage at a frequency between 0.01 Hz and 100 kHz with an amplitude of 0.5 mV. This technique was employed to identify the ions by monitoring the current as a function of time upon application of a fixed DC voltage (0.8 V) across the sample, which was sandwiched between two stainless steel electrodes. The Watanabe technique was used in this characterization of H^+ using MnO_2 as a blocking electrode.

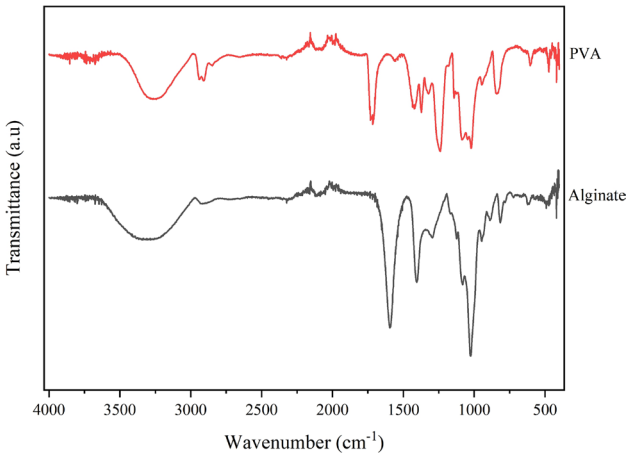

Fig. 2 FTIR for pure PVA and alginate.

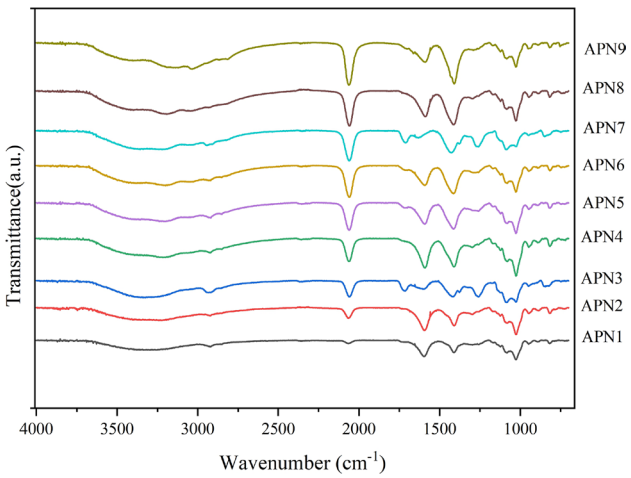

Fig. 3 FTIR spectra of SPE system (Al–PVA–NH_4SCN) in the wavenumber range of 700–4000 cm^{-1}.

Results and Discussion

Infra-Red (IR) Analysis

The FTIR study in this work provided crucial insights into the composition of the blend and the interactions between the polymers, which likely occur due to hydrogen bonding or complex formation. Figure 2 presents the infrared spectra of the pure PVA and alginate in powder form, and Fig. 3 presents the Al–PVA–NH_4SCN system with varying weight percentages of NH_4SCN, spanning wavenumbers from 700 to 4000 cm^{-1}.

In Fig. 2, the characteristic bands for the alginate and PVA are identified at 3341 cm^{-1} (OH stretching), 1590 cm^{-1} (asymmetric -COO^- stretching), and 1407 cm^{-1} (symmetric -COO^- stretching) [8]. The vibrational frequency at 3425 cm^{-1} is assigned to the hydroxyl (OH) band plane bending, indicating potential hydrogen bonding during the complexation of the system. The interactions between the carboxylate group (-COO^-), hydroxyl group (–OH), and glycoside bond (C-O-C) are crucial for the blend's structural integrity, thereby optimizing the performance of the SPEs. The functional groups expected to participate in these interactions based on entire FTIR spectra in Fig. 3 are highlighted in Fig. 4.

The bands at 1738 cm^{-1}, 1644 cm^{-1}, and 1267 cm^{-1} are attributed to the C=O, C=C, and C-O-C vibration modes of the acetate group from the PVA host polymer, respectively [9]. Despite the 85% hydrolysis of PVA, the presence of these bands suggests incomplete hydrolysis of polyvinyl acetate during PVA production [2]. The shifting of peaks and changes in intensity indicate the formation of complexes between the Al–PVA blend and NH_4SCN. In Fig. 4(b), new peaks with varying intensities appear at 2061 cm^{-1} across different NH_4SCN-doped films, corresponding to

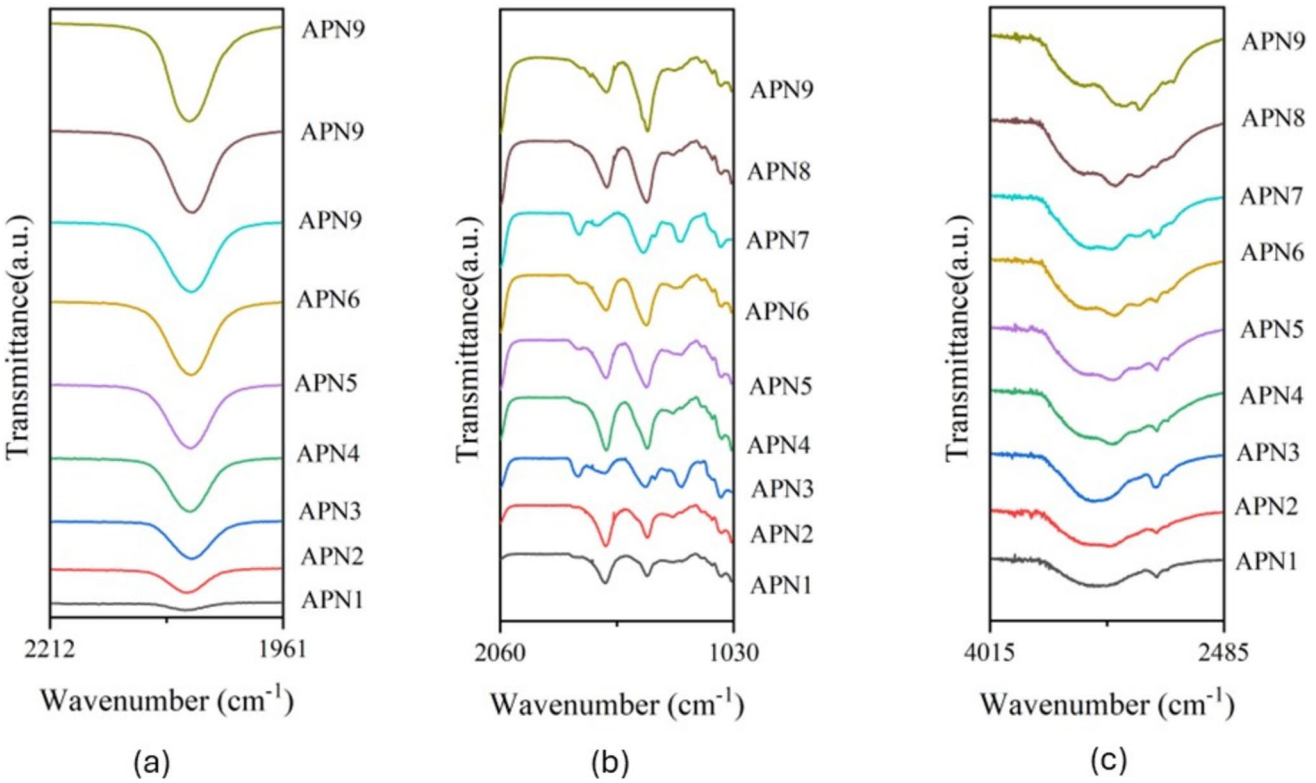

Fig. 4 FTIR spectra at the different wavenumber ranges: (a) 2060–1040 cm^{-1}, (b) 2201–1963 cm^{-1}, and (c) 4000–2500 cm^{-1}.

the aromatic SCN^- stretching of NH_4SCN [12]. SCN^- is an ambident linear anion with two alternative reactive sites, capable of forming N-bonding (CN stretching), S-bonding (CS stretching), and bridge complexes involving the S and N atoms (SCN bending) [13]. The strong intensity of the SCN^- stretching mode in Fig. 4(a) makes it a suitable candidate for studying ion association effects in SPEs [11, 14, 15].

When NH_4SCN is introduced into the blend, significant changes are observed in the FTIR spectra. In Fig. 4(c), two peaks in the 3000–3600 cm^{-1} range, corresponding to symmetric and asymmetric vibrations of NH_4^+, overlap with the -OH band of the Al–PVA blend [10]. This overlap suggests potential interactions between NH_4^+ ions and the hydroxyl groups in the blend. The shift in OH stretching frequency from 3341 cm^{-1} in the pure Al–PVA to lower frequencies in the doped samples (e.g., 3425 cm^{-1} in APN1) indicates hydrogen bonding between NH_4^+ ions and hydroxyl groups in the polymer matrix [16]. This interaction is further supported by the increased intensity and broadening of the -OH band with higher NH_4SCN concentrations, reflecting stronger hydrogen bonding and protonation effects. Ahmed et al. [17] reported that salt–polymer interactions can be observed from the band shifts. As shown in Fig. 4(c), the -OH band shifts to higher frequencies with increasing salt concentration, indicating complexation between the Al–PVA blend and NH_4SCN. Noor et al. [9] observed a similar phenomenon when lithium bis(oxalate)borate was added to PVA, indicating interaction between the salt's cation and the oxygen atom of the polymer host's -OH group.

According to Fuzlin et al., ion conduction in this region occurs via the Grotthuss mechanism, facilitated by proton migration (H^+) within the polymer matrix [11, 18]. This mechanism involves the coordination interaction of the carboxylate ($-COO^-$) moiety of alginate with the H^+ ion from the NH_4^+ substructure in NH_4SCN, triggering protonation between the cation (H^+) and the carboxylate group of alginates [19, 20]. Increasing the ionic dopant concentration leads to an increase in peak intensity from APN1 to APN9. In this system, the NH_4^+ cation functions as an electrophile, showing affinity for the coordinating site (oxygen) of the carboxylate anion from the alginate, thereby enhancing ionic conductivity and the electrochemical properties of the SPE system [21, 22]. These results suggest that the Al–PVA interaction occurs through (1) hydrogen bonding between the OH group of PVA and the -OH and ether groups of Al, and (2) hydrogen bonding between the -OH group of Al and the C=O and C-O groups of PVA.

The strong intermolecular interactions leading to protonation and deprotonation in the SPE system likely contribute to enhanced structural integrity and charge carrier movement via ion hopping, as illustrated in Fig. 5. During the ion-hopping mechanism, labile bonds form between NH_4SCN with a

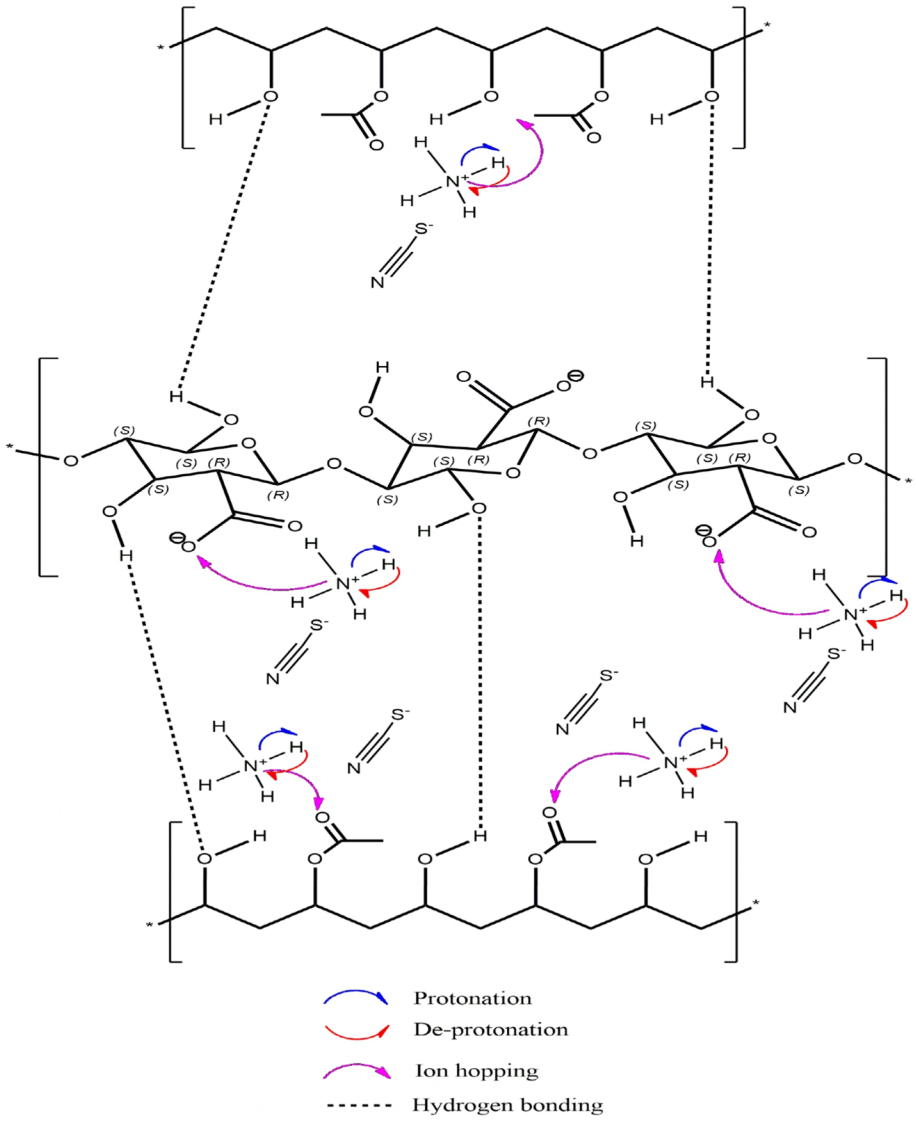

Fig. 5 Schematic of proton hopping in the SPE system.

lower energy threshold, creating alternative pathways for ion movement. These labile bonds, characterized by their low energy requirement for dissociation and reformation, facilitate effective ion hopping over shorter distances, improving ion transport. Similar findings were reported by Hafiza and Isa [23], who noted that the compatibility between polymer complexes and NH_4SCN as dopants significantly affected the ion-hopping pathway, thereby increasing ionic conductivity.

Thermal Properties

The thermal properties of the Al–PVA–NH_4SCN SPE system were determined using TGA. Figure 6 shows the thermograms for multiple samples labeled APN1–APN9, plotting the weight percentage against temperature. The TGA curves are divided into three distinct stages of weight loss in the temperature range of 30–800 °C under an N_2 atmosphere, with the details tabulated in Table II.

In the first stage (up to ~ 150 °C), all the samples exhibit minor weight loss, likely due to the evaporation of adsorbed moisture and volatile components, a common phenomenon observed in TGA studies of polymeric materials [12]. The minimum weight loss was observed in APN9 (8.38%) compared to APN7 (13.35%).

The second stage (~ 150 °C to ~ 300 °C) exhibit significant weight loss for all the samples, attributed to the thermal degradation of the carboxylate group ($-COO^-$) from the polymer backbone, which consists of alginate and PVA. APN7 exhibits a weight loss of about 44% with a decomposition temperature of 322.34 °C. This stage is critical, as it highlights the main decomposition temperature range where the polymer chains break down into smaller, volatile molecules, a common characteristic of polymer decomposition under thermal stress. According to the FTIR analysis, the alginate consists of the major structure of the carboxylate group in the polymer matrix and readily undergoes

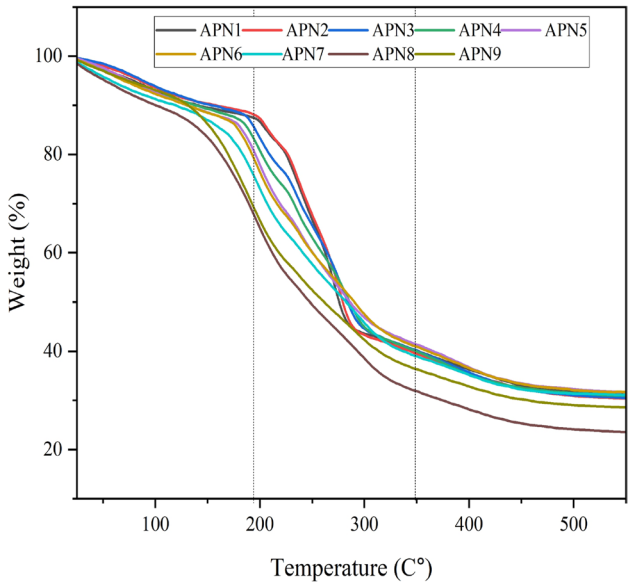

Fig. 6 TGA thermograms of Al–PVA–NH_4SCN.

decarboxylation (degradation) at 219–261 °C. The addition of the ionic dopant to the polymer backbone facilitates dissociation upon heating, where more protonation (H +) from NH_4SCN occurs as it is attracted to the -COO− group of the alginate backbone. This interaction increases the decomposition temperature and reduces the weight loss of the SPE system. The weight loss reduction in APN2 (43.44%) indicates that APN7 has an intense amorphous phase in the structure, enhancing the SPE system's heat sensitivity. This suggests an enhancement of thermal stability, with fewer monomers detaching from the polymer backbone due to the complexation of Al–PVA–NH_4SCN in the SPE system [13].

In the third stage (~ 300 °C to ~ 500 °C), further weight loss continues, possibly due to the breakdown of more stable polymer structures or residual materials. The curves for APN1 to APN9 show similar trends, with variations in the onset and extent of weight loss across the stages. APN8 and APN9 exhibit the most substantial weight loss in the second stage, indicating lower thermal stability compared to the other samples. By the end of the temperature range (~ 500 °C), all the samples converge to a residual weight percentage between 10% and 20%, representing the non-volatile components or inorganic residues left after thermal decomposition. The correlation between the thermal stability and ionic conductivity of the samples can be inferred from the weight loss data. Samples with lower weight loss, such as APN7, are expected to exhibit higher ionic conductivity, which is because the stronger structural integrity and reduced degradation at elevated temperatures suggest more efficient ion transport pathways within the polymer matrix [14]. The improved thermal stability, resulting from the interactions between NH_4SCN and the polymer matrix, enhances the overall performance of the SPE system. This TGA analysis demonstrates the thermal stability of the Al–PVA–NH_4SCN system, showing how the incorporation of NH_4SCN influences the decomposition behavior and stability of the polymer electrolytes, which is crucial for achieving higher ionic conductivity.

Crystallinity Analysis

Figure 7(a) illustrates the plot for the raw materials, PVA and alginate. The PVA spectra show a crystalline peak at 20°, and, for the alginate, a semi-crystalline hump is observed at 25-45°. On the other hand, Fig. 7(b) displays the XRD patterns of the Al–PVA–NH_4SCN SPE system with varying NH_4SCN compositions. In the spectrum of APN1, two diffraction peaks at 10.13° and 20.12° indicate the semi-crystalline structure of the SPEs, attributed to typical polysaccharide linkages. According to Hodge et al. [15], the amorphous nature of a polymer matrix can be inferred from the peak intensity and degree of crystallinity. The addition of NH_4SCN reduces the intensity of these peaks, with a shift to higher angles observed from APN1 to APN9. The disappearance of sharp peaks indicates that the dopant systems are completely dissociated within the polymer matrix [16], suggesting complexation between NH_4SCN

Table II Thermal properties of Al–PVA–NH_4SCN

Sample	Maximum temperature (°C)			Weight loss (%)		
	1 st stage	2nd stage	3rd stage	1 st stage	2nd stage	3rd stage
APN1	196.80	290.20	459.43	12.31	42.54	12.17
APN2	199.93	291.22	478.90	12.10	43.44	12.41
APN3	188.12	295.05	457.50	11.48	43.75	12.10
APN4	181.40	303.83	558.00	12.55	42.53	13.50
APN5	174.55	314.52	444.75	13.18	41.58	12.75
APN6	176.47	321.38	463.26	12.75	43.25	11.86
APN7	163.86	322.34	452.61	13.35	44.84	9.96
APN8	141.51	318.51	461.35	11.13	53.06	10.32
APN9	140.9	310.37	547.83	16.26	48.11	11.2

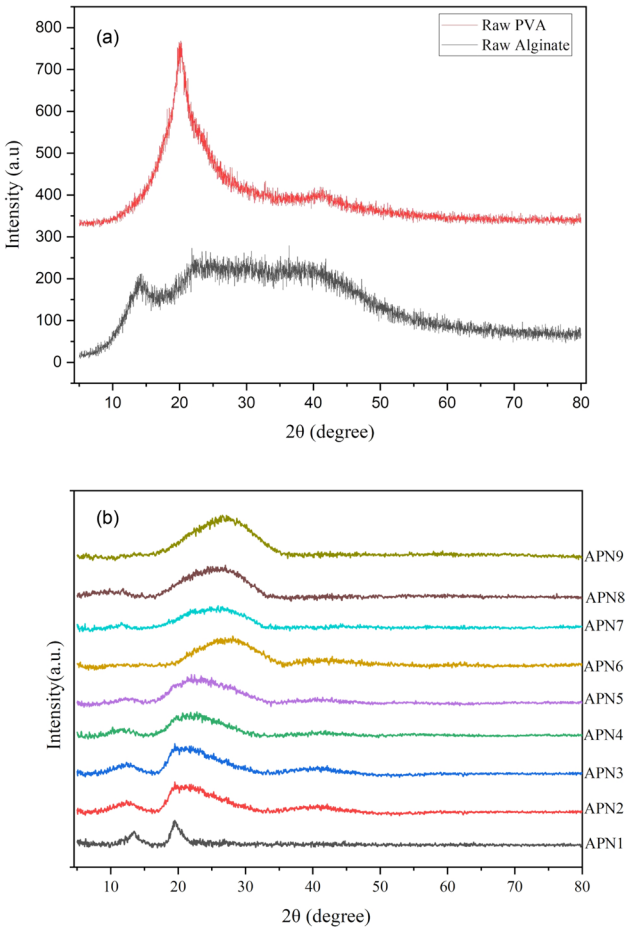

Fig. 7 XRD spectra of (a) raw PVA and alginate and (b) Al–PVA SPE system doped with various NH_4SCN.

and the Al–PVA polymer blend, resulting in an increased amorphous hump [11]. The maximum amorphous nature of the polymer membrane facilitates the protonation of H^+ to the Al–PVA backbone by providing more oxygen vacant sites, thereby improving ionic conductivity significantly [17, 18]. Based on the XRD results, the APN7 sample exhibits a highly amorphous nature with no noticeable peaks, which is expected to enhance its ionic conductivity. However, the amorphous phase starts to decrease in sample APN8, possibly due to the inability of the alginate host polymer to accommodate higher NH_4SCN concentrations, leading to reduced transport properties and ionic conductivity [19, 20].

Figure 8 displays SEM micrographs of the electrolytes. The surface of APN1 is rough with phase separation, indicating that the PVA and alginate are miscible and homogeneously blended. Although both the PVA and alginate are semicrystalline in nature, the blending process and subsequent salt doping significantly disrupt the crystalline domains. This disruption facilitates the formation of interconnected amorphous regions, which manifest as a porous morphology under SEM. The addition of NH_4SCN salt transforms the morphology of the Al–PVA–NH_4SCN blend into a more porous structure. The generation of porosity is attributed to several factors: (1) ionic interaction between the polymer chains and the salt induces structural loosening, creating microvoids; (2) evaporation of residual solvent during drying enhances pore formation; and (3) the plasticizing effect of NH_4^+ and SCN^- ions further suppresses crystallinity, promoting a more open morphology. The porosity of polymer electrolytes strongly influences ionic transport, promoting increased conductivity [21]. As more NH_4SCN is incorporated into the Al–PVA–NH_4SCN host, the number and size of the pores increase, suggesting that the addition of salt promotes pore formation, which provides pathways for ion hopping and ionic mobility, thereby enhancing ionic conduction.

The surface of APN7 exhibits the largest pore size, confirming its status as the highest-conducting electrolyte in this study. Beyond APN8, the surface of the electrolytes becomes rough with the appearance of agglomerates and separation. This deterioration in microstructure is due to oversaturation of salt content, leading to salt recrystallization and agglomeration as seen in the SEM micrograph (APN9). This observation is attributed to the formation of ion associations, as discussed in the FTIR analysis. The increased ion association rate leads to agglomerate formation, which blocks ion conduction and decreases conductivity [2]. The SEM images confirm the morphological evolution from uniform roughness to porosity and finally to phase segregation with salt clusters. The SEM images reveal the homogeneity of the rough surface, without phase separation, likely due to the setups in the polymer electrolyte enhancing proton transport (Arof et al., 2011) [24].

The morphology observed in the SEM images aligns with the XRD analysis, suggesting that there is less dissolution of salt in the polymer matrix at higher loadings. The XRD and SEM analyses together provide a comprehensive understanding of the impact of NH_4SCN doping on the crystallinity and morphology of the Al–PVA–NH_4SCN SPE system. The increase in amorphous content with higher NH_4SCN concentrations, evidenced by the broadening of XRD peaks and the rougher surface morphology observed in SEM images, suggests that NH_4SCN effectively disrupts the crystalline structure of the polymer matrix, which enhances the ionic conductivity by providing more free volume and facilitating the transport of ions. The correlation between the increased amorphous phase and the improved ionic conductivity is consistent with the thermal stability findings from the TGA analysis. Samples with higher NH_4SCN content, which exhibit lower weight loss and higher thermal stability, also demonstrate enhanced ionic conductivity due to their more amorphous structure. This comprehensive analysis highlights the importance of optimizing NH_4SCN concentration to strike a balance between thermal stability,

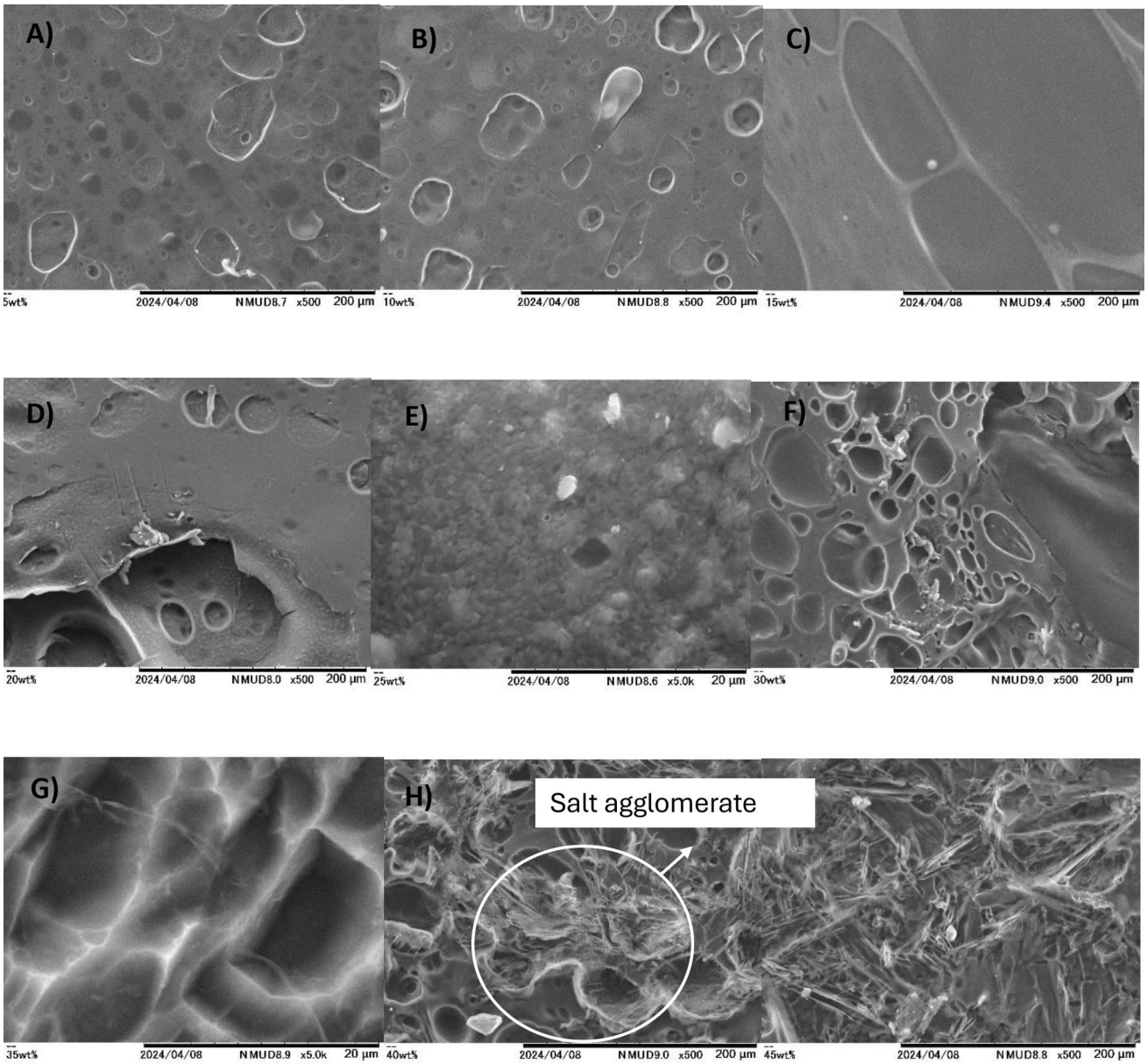

Fig. 8 Surface morphology of (A) APN1, (B) APN2, (C) APN3, (D) APN4, (E) APN5, (F) APN6, (G) APN7, (H) APN8, and (I) APN9 at ×500–0.5 K magnification.

morphological characteristics, and ionic conductivity in SPE systems.

Ionic Conduction Analysis

The resultant impedance plots, corresponding to the fitting of the experimental and theoretical data for the selected samples of the SPE system, are illustrated in Fig. 9. The bulk resistance (R_b) can be determined from the intercept of the high-frequency semicircle and the low-frequency spike on the Z_r axis [25]. The appearance of the semicircle at high frequencies in the data suggests a combination of R_b and a CPE. The CPE can be described as a"leaky capacitor,"meaning it does not behave like a perfect capacitor, indicating that NH_4^+ ions are migrating within the polymer matrix [26]. The presence of R_b could be due to the immobility of polymer chains. Additionally, the interface between the electrode and the electrolyte acts as a capacitor, because the stainless-steel stage serves as a blocking electrode, preventing charge transfer at the interface. The real and imaginary impedance of the bulk capacitance can be described using [27]:

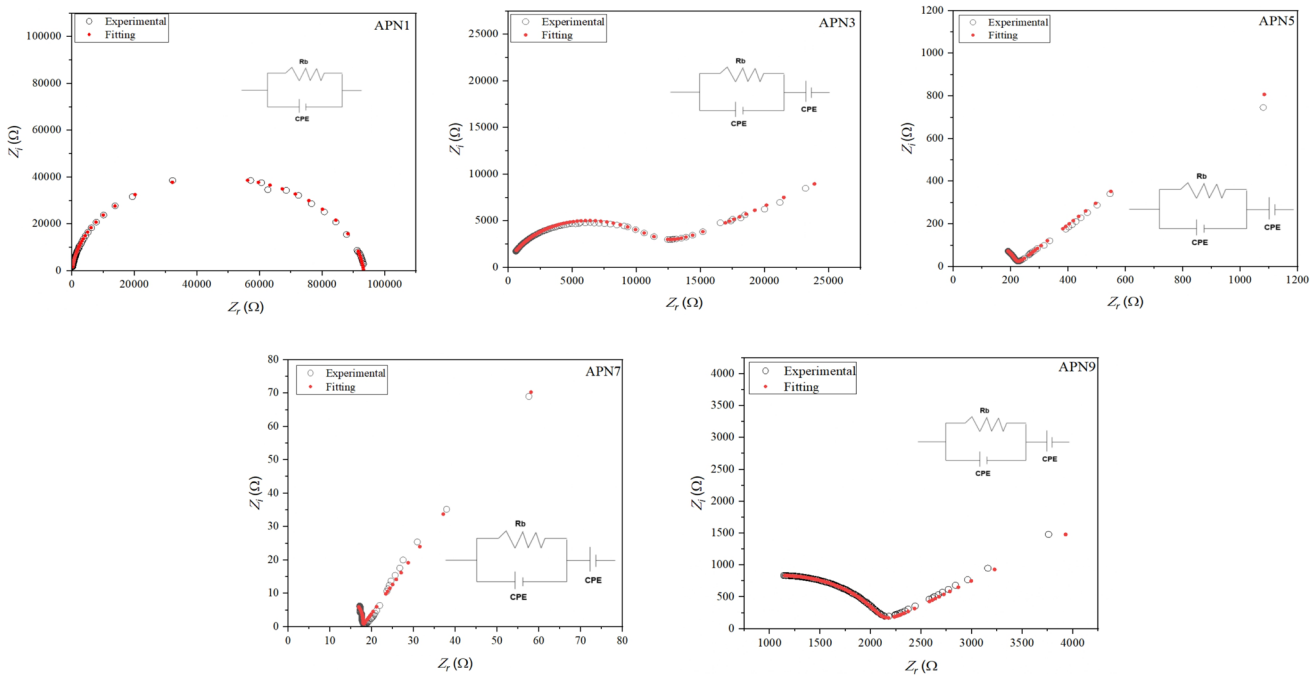

Fig. 9 Impedance plot for the selected samples of the Al–PVA–NH_4SCN SPE system.

$$Z_r = \frac{\cos\left(\frac{\pi p}{2}\right)}{k^{-1}\omega^p} \tag{8}$$

and

$$Z_I = \frac{\sin\left(\frac{\pi p}{2}\right)}{k^{-1}\omega^p} \tag{9}$$

The relationships between the real and imaginary parts of the impedance plot, composing a semicircle and a spike, are given by:

$$Z_r = \frac{R + R^2 {k_1}^{-1}\omega^{p1}\cos\left(\frac{\pi p_1}{2}\right)}{1 + 2R{k_1}^{-1}\omega^{p_1}\cos\left(\frac{\pi p_1}{2}\right) + R^2 {k_1}^{-2}\omega^{p_1}} + \frac{\cos\left(\frac{\pi p_2}{2}\right)}{{k_2}^{-1}\omega^{p_2}} \tag{10}$$

$$Z_I = \frac{R^2 {k_1}^{-1}\omega^{p1}\sin\left(\frac{\pi p_1}{2}\right)}{1 + 2R{k_1}^{-1}\omega^{p_1}\cos\left(\frac{\pi p_1}{2}\right) + R^2 {k_1}^{-2}\omega^{p_1}} + \frac{\sin\left(\frac{\pi p_2}{2}\right)}{{k_2}^{-1}\omega^{p_2}} \tag{11}$$

According to Fig. 9, the semicircle formation resulting from the addition of NH4SCN is connected to the relaxation process in bulk SPEs, which contributes to a decrease in ionic conductance. In Fig. 9, the combination of an inclined spike and a semicircle indicates semiconducting capabilities, as observed in APN3–APN9 [28]. Arof et al. [29] stated that the inclination spike and the semicircle's interception with the real axis were used to determine the R_b value. In contrast, APN7 exhibited only an inclined spike with an incomplete semicircle that approached the inclined spike, indicating improved ionic conduction involving free ions and, thus, higher ionic conductivity [30]. Additionally, semicircles reappear more prominently in APN9, which has been linked to salt aggregation, resulting in the crystalline characteristics of the SPEs, as shown by XRD and SEM studies. Salt aggregation, which leads to a reduction in free ions, may cause a sudden decrease in ionic conductivity and ionic mobility.

The parameters p_1, p_2, C_1, and C_2 were determined using impedance plot fittings, as described by other researchers and shown in Table III [31, 32]. Here, p_1 refers to the ratio of the angle between the diameter of the semicircle, and p_2 is the skew parameter that controls the degree of the inclined spike [33]. Our calculations show that the experimental R_b values are consistent with the data generated from the fittings. Furthermore, the APN7 sample, with the lowest R_b value, was inferred to have the highest ionic conductivity. On the other hand, the p_2 value is within the range of $0 < p < 1$, indicating that, in this present system, the spike inclination was less than 90°, suggesting that both capacitive and resistive properties are present in the samples.

Figure 10 illustrates the ionic conductivity of Al–PVA–NH_4SCN polymer blends with varying NH_4SCN compositions. The samples were sandwiched between two stainless-steel blocking electrodes to measure the electrical properties of the system. Previous work by Ghazali et al.

Table III Parameters of the equivalence circuit for SPE system

Sample	R_b (Ω) Experimental	R_b (Ω) Theoretical	p_1	C_1	p_2	C_2
APN1	91,866.00	93,204.5	0.95	2.85E−10	…	…
APN2	21,086.00	12,572.2	0.40	3.29E−06	0.88	5.88E−10
APN3	10,106.00	12,601.5	0.44	2.00E−06	0.89	5.63E−10
APN4	1276.00	1336.66	0.61	3.84E−08	0.48	1.14E−05
APN5	197.00	226.789	0.90	4.50E−04	0.50	5.02E−05
APN6	202.1	208.839	0.16	1.38E−05	0.60	2.36E−05
APN7	18.88	18.0751	1.10	5.10E−10	0.66	2.65E−04
APN8	1124.00	1119.53	0.94	5.11E−10	0.41	4.83E−05
APN9	2183.00	2177.01	0.89	4.23E−10	0.42	3.66E−05

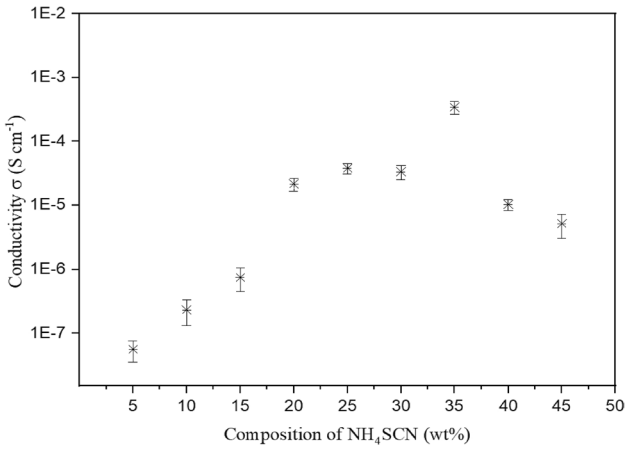

Fig. 10 The ionic conductivity plot of various NH_4SCN contents.

revealed that the Al–PVA polymer blend exhibited a room-temperature conductivity value of approximately 4×10^{-8} S cm^{-1} [23]. The conductivity increases with the addition of NH_4SCN, reaching an optimal value of 3.42×10^{-4} S cm^{-1} at 35 wt% (APN7). However, for APN6, the conductivity drops to 8×10^{-5} S cm^{-1}, despite a higher number of charge carriers. This suggests that ion mobility plays a crucial role in determining the conductivity.

The observed drop in conductivity for APN6 could be due to the increased formation of ion pairs or clusters, which reduces the number of free ions available for conduction and leads to decreased conductivity [34]. Additionally, the microstructure of the electrolyte might become less favorable for ion transport, possibly due to phase separation or the formation of a less conductive network [25]. In contrast, APN7 exhibits the highest conductivity, indicating an optimal balance between charge carrier concentration and ion mobility. At this stage, the ionic dopant might lead to a reorganization of the microstructure, creating more continuous and better-conducting pathways, thereby enhancing ionic conductivity. The improvement in ionic conductivity at this stage is likely due to the increased availability of ions for migration. The presence of NH_4^+ in the SPE system releases free ions (H^+), which interact with the polar groups in the biopolymer blend, thereby enhancing conductivity.

The findings of ionic conductivity reveal a clear correlation between the NH_4SCN content, the structural properties of the polymer matrix, and the ionic conduction behavior. The optimal NH_4SCN concentration (35 wt%) maximizes ionic conductivity by enhancing the amorphous nature of the polymer and creating efficient pathways for ion transport. This is corroborated by the XRD and SEM analyses, which reveal an increase in amorphous content and larger pore sizes within the polymer matrix at this concentration. The decrease in ionic conductivity at higher NH_4SCN concentrations is attributed to the formation of ion pairs or aggregates, which obstruct the conduction pathways. This highlights the importance of optimizing the dopant concentration to balance the enhancement of amorphous content and the prevention of ion aggregation.

Figure 11 illustrates the temperature dependence of the ionic conductivity of the SPE samples. The data indicate that, as the temperature increases, the ionic conductivity also increases. This can be attributed to the dissociation of protons from NH_4^+ ions when they gain sufficient energy, releasing a large number of ions into the system and increasing ionic conductivity [35]. Additionally, the temperature-induced increase in ionic conductivity leads to an expansion in free volume, which enhances segmental motion and charge mobility as the polymer chains acquire enough energy to vibrate and move between sites [36]. At elevated temperatures, the polymer chains vibrate, causing bond rotations and weakening interactions within the SPE. This process facilitates the movement of H^+ ions from NH_4SCN towards the coordinated groups in the Al–PVA backbone. The temperature dependence of the ionic conductivity further elucidates the conduction mechanism, with lower activation energies observed for samples with higher NH_4SCN content, indicating that the amorphous structure facilitated by NH_4SCN doping reduces the energy barrier

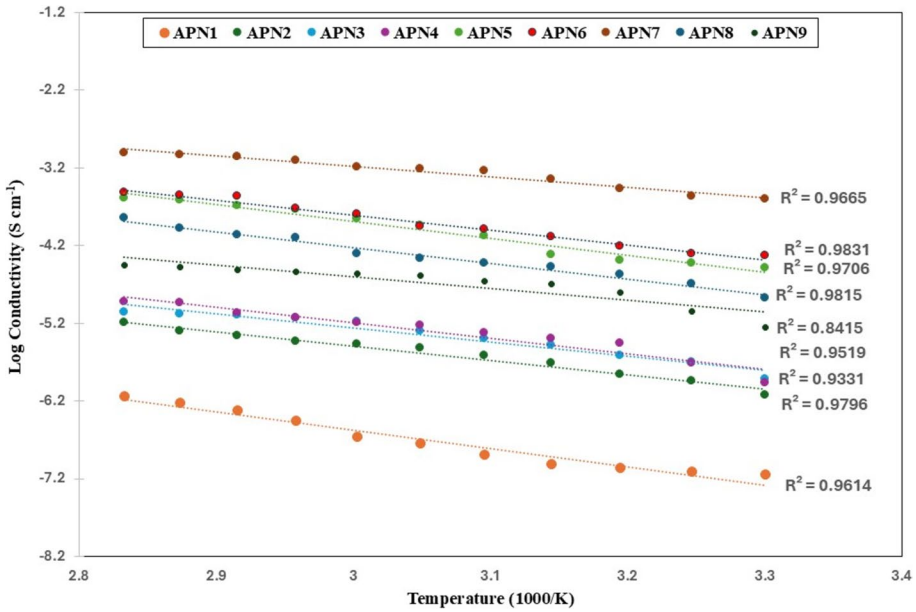

Fig. 11 Different temperature study on SPE.

for ion transport, enhancing the overall ionic conductivity of the SPE system.

Furthermore, the stable ionic conductivity values during heating suggest that the water content does not significantly influence the enhancement of ionic conductivity; instead, it is the H^+ ions from NH_4SCN that impact it. SPE samples showed high R^2 values close to unity (R^2 ~1), indicating adherence to the Arrhenius behavior [37]. Samples APN2 to APN8 exhibit high R^2 values (above 0.95), indicating a strong linear relationship between log conductivity and the inverse temperature. APN9 exhibits the lowest R^2 value, indicating the least linearity in its conductivity response to temperature changes [38]. This significant deviation may be due to a more heterogeneous distribution of the dopant within the polymer matrix or the presence of impurities that affect the conductivity measurements. Additionally, APN9 might have structural anomalies or phase separation that disrupt the linear relationship between temperature and conductivity [39].

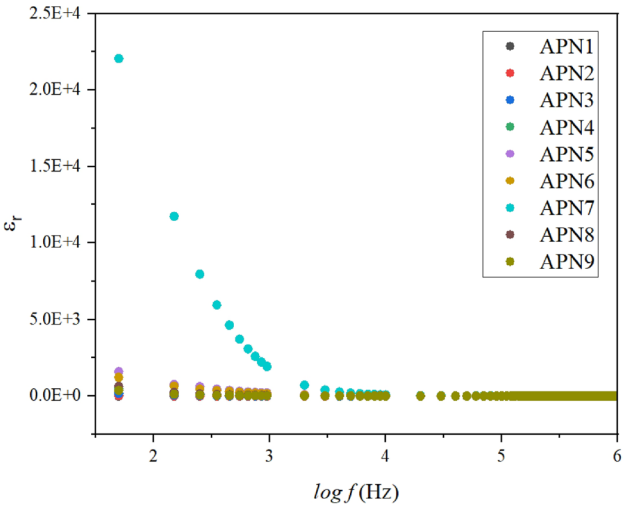

Fig. 12 The dielectric constant of SPE.

Transport Properties of SPE System

The dielectric properties of any system can be characterized by frequency-dependent parameters, which the complex permittivity can define as ε. The complex permittivity or dielectric constant of a system is defined by $\varepsilon^* = \varepsilon_r - j\varepsilon_I$. The real and imaginary parts of complex permittivity are of particular significance for an ion-conducting polymer. Figure 12 shows the frequency dependence of the real part of the complex permittivity at different concentrations of the SPE system at room temperature, which indicates that the low-frequency dispersions are very strong and can be attributed to space charge polarization effects arising from the electrodes, as observed for APN7. The samples with optimal NH_4SCN content demonstrate an optimal balance of charge mobility. In the high-frequency region, due to the high periodic reversal of the field at the interface, the contribution of charge carriers towards the dielectric constant decreases with increasing frequency. The dielectric loss occurs due to collisions between mobile charge carriers.

The transport properties for the SPE system were evaluated from the impedance analysis. To obtain the values of the dielectric constant, ε, the real part of complex permittivity, ε_r, was plotted in Fig. 13 and substituted in Eq. (2). The calculated dielectric constant was employed in Eqs. (4–6) [24]. The transport parameters of the SPE system were plotted as a function of NH_4SCN contents using Nova and OriginPro

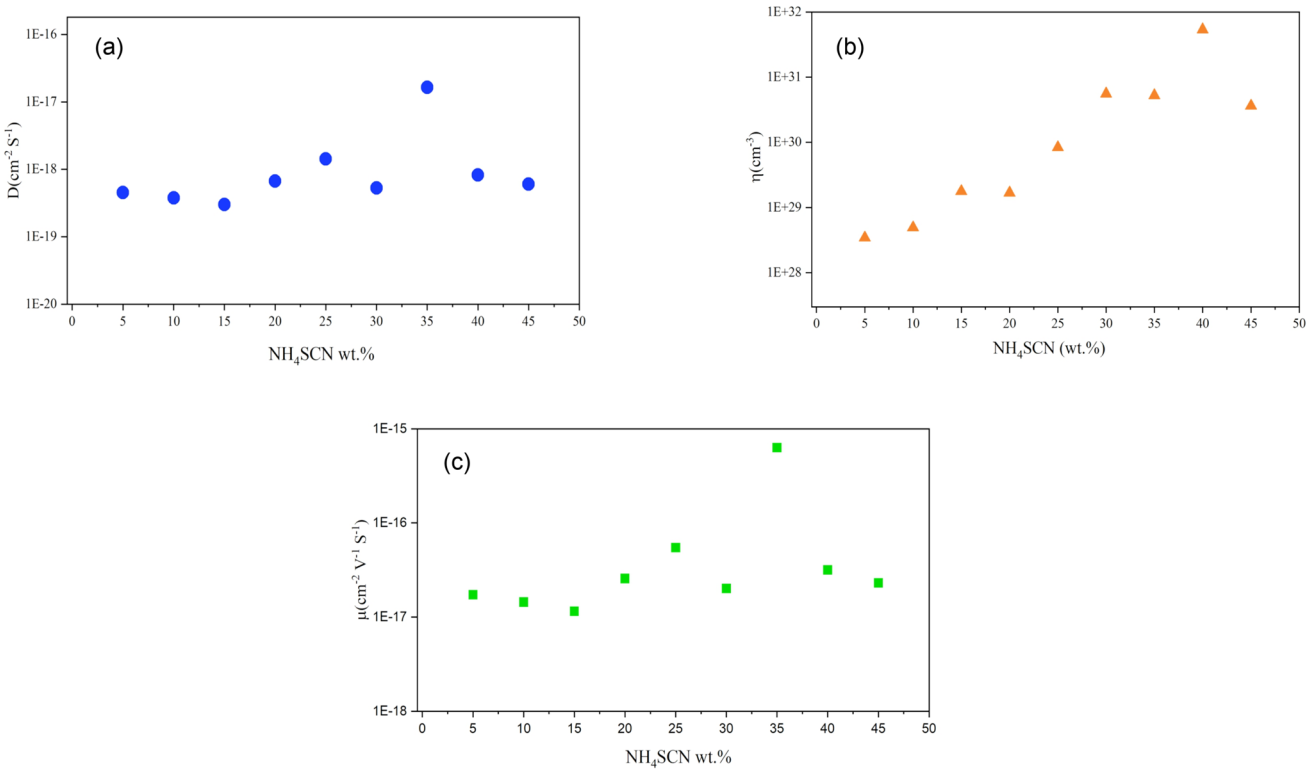

Fig. 13 Plots of (a) diffusion coefficient (D), (b) charge carrier number density (η), and (c) charge carrier mobility (μ).

2022 software are shown in Fig. 13, which depicts the ion mobility (μ) and the diffusion coefficient (D) showing a similar trend with ionic conductivity where it rises sharply at APN7 and drops at APN8. This behavior follows the trend of conductivity-composition in the SPE system. The maximum ionic conductivity of Al–PVA doped with 35 wt% of NH_4SCN (APN7) exhibits maximum μ and D values of 6.13×10^{-16} cm^2 V^{-1} s^{-1} and 1.65×10^{-17} cm^2 s^{-1}, respectively. The dissociation of H^+ ions from NH_4^+ explains the increased number of ions, leading to an increased ionic conductivity in the SPE system. Additionally, the diffusion of ions, D, in the polymer matrix contributes to the increase in ionic conductivity, as the movement of ions in the SPE system can easily interact. Furthermore, this can be shown by increasing D and μ until they reach the ideal composition, which corresponds to the ionic conductivity [40].

Notably, the number density (η) of ions has increased linearly with the composition of NH_4SCN, indicating an increase in ion occurrence. The highest value of η is 3.61×10^{31} cm^{-3}, contrasting with the ionic conductivity due to the APN9 being higher than the optimum composition of NH_4SCN at APN7. The increase in η inferred that the NH_4SCN in the polymer matrix was too heavy, contributing to a decrease in ion mobility (μ) and diffusion coefficient (D), which was affected by the formation of ion clusters and overcrowding of mobile ions (H^+). In addition, the addition of NH_4SCN in the SPE system confirmed the conjecture from the FTIR study, where the H^+ from -OH jumps to the lone pair of -COO^- from the polymer backbone. The transport properties and conductivity are enhanced due to the flexibility of the segmental motion of the polymer chains in the SPE system, which is crucial for the enhancement of the SPE.

Transference Number (TN) Studies

Transference number (TN) measurements were conducted to determine the contribution of the SPE system to the overall ionic conductivity. This study aims to determine whether the conductive sample is more cationic, anionic, or otherwise [41]. The ionic transference number, or ion value, must be higher than 0.5, along with its ionic conductivity. For the normalized polarization current versus time, the TN can be calculated by:

$$t_{ion} = \frac{I_i - I_f}{I_i} \tag{12}$$

where I_I is the initial current and I_f is the final current.

Figure 14 shows the plot of normalized polarization against time. Initially, the total current decreases as the time increases, until it reaches a constant state (final total current).

At a constant state, the ionic species achieve a depleted state when the ions are polarized and scattered, which might be due to the ionic current passing through the ion-blocking electrode rapidly decreasing over time if the electrolyte has an optimum ionic concentration [42]. For sample APN7, the $t_{ion} = 0.88$ was achieved, indicating that the ionic conduction is mainly ions, primary due to a TN close to ~ 1.

The possible ionic mobility will occur due to the proton number of H^+ from NH_4SCN. To determine the proton TN, impedance measurements and TN measurements were used in this work. Impedance measurements determined the contact resistance before and after potential polarization [41]. Figure 15 shows the impedance before and after polarization for the sample APN7 using the reversible electrode, for which manganese (MnO_2) was chosen since the proton (H^+) is expected to be mobile in the polymer matrix. The electrolyte was placed between two electrodes reversibly, much like a sandwich. To investigate the H^+ TN, the Bruce and Vincent [25] method was used as in:

$$t_H^+ = \frac{I_{ss}(\Delta V - I_o R_o)}{I_o(\Delta V - I_{ss} R_{ss})} \tag{13}$$

where R_o corresponds to the bulk resistance before, R_{ss} is the bulk resistance after, I_o is the initial current, I_{ss} is the current at the constant state, and ΔV is the applied potential. Since no redox reaction was involved, the cation will primarily contribute to the total current while the anion vanishes (Bruce). The plot in Fig. 15 reveals the R_o to be 809,584 Ω and R_{ss} to be 1,232,610 Ω. On the other hand, the value for I_o was 4.9 μA, I_{ss} was 0.6 μA, and the H^+ion TN was 0.66.

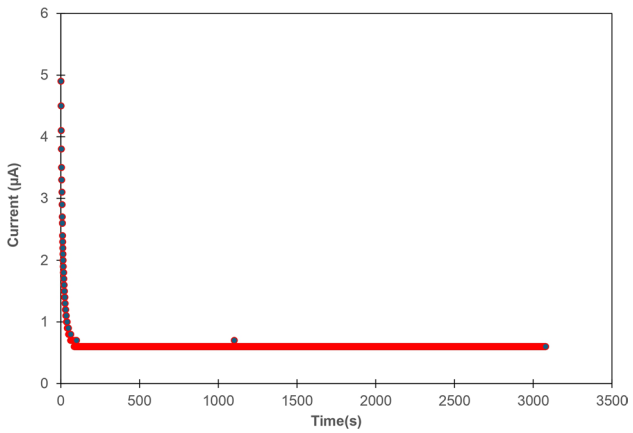

Fig. 14 Normalize polarization current versus time for sample APN7.

Conclusions

An electrolyte system using an Al–PVA polymer blend as the host and NH_4SCN as the doping salt was successfully prepared via the solution-casting technique. FTIR analysis revealed significant interactions, particularly through hydrogen bonding, which facilitated increased ion dissociation and enhanced ionic conductivity, reaching an optimal value of 3.4×10^{-4} S cm^{-1} in the sample containing 35 wt% of NH_4SCN (APN7). The temperature-dependent ionic conductivity of all the SPE systems followed Arrhenius behavior, indicating thermally-assisted ion transport, with regression values close to unity. TGA analysis demonstrated good thermal stability, which, along with enhanced amorphous phases observed in XRD and SEM analyses, contributed to the favorable conductivity results. The incorporation of

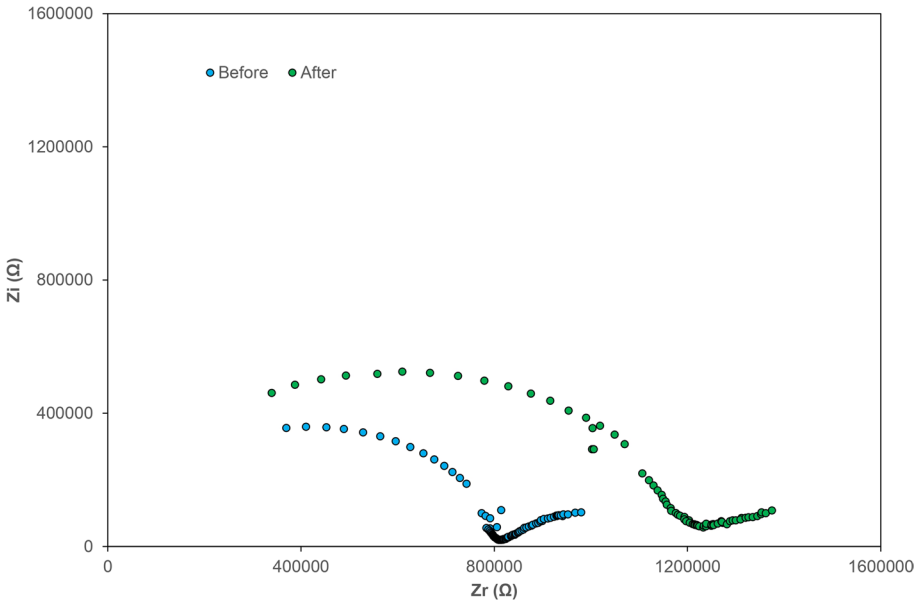

Fig. 15 Impedance measurement before and after polarization for sample APN7.

NH_4SCN improved both the diffusion coefficient and ion mobility, correlating well with the observed ionic conductivity. Lastly, from the TNM analysis, we obtained values of 0.88 near 1 and an H^+ value of 0.66, indicating that ionic conductivity is predominantly due to cationic conduction. Overall, the Al–PVA–NH_4SCN biopolymer-based SPE system shows significant potential for application in electrochemical devices, demonstrating strong conducting properties and robust thermal stability.

Acknowledgment The authors would like to thank Ministry of Higher Education Malaysia (MOHE) under the FRGS fund (FRGS/1/2023/STG05/UMP/02/2) and University Malaysia Pahang Al-Sultan Abdullah (UMPSA) under the UMPSA Distinguish Grant (RDU233001) for funding this research and Japan Advanced Institute of Science and Technology (JAIST), for the help and support given for the completion of this work. The authors would also like to thank Ionic Materials Team members, M.A. Saadiah and N.F. Mazuki, thank you for kindly helping me complete this research.

Funding Open access funding provided by The Ministry of Higher Education Malaysia and Universiti Malaysia Pahang Al-Sultan Abdullah. The present work was funded by the Ministry of Higher Education Malaysia (MOHE) under the FRGS fund (FRGS/1/2023/STG05/UMP/02/2) and University Malaysia Pahang Al-Sultan Abdullah (UMPSA) under the UMPSA Distinguish Grant (RDU233001).

Conflict of interest The authors declare that they have no conflict of interest.

References

1. Y.W. Foong, K. Lian, D. Kirk, and S. Thorpe, Borotungstic Acid: Polyacrylamide Solid Electrolytes for Electrochemical Capacitors with H_3PO_4 Plasticizer. *Mater. Sci. Eng. B* 229, 96–104 (2018). https://doi.org/10.1016/j.mseb.2017.12.019.
2. N.A. Shamsuri, S.N.A. Zaine, Y.M. Yusof, W.Z.N. Yahya, and M.F. Shukur, Effect of Ammonium Thiocyanate on Ionic Conductivity and Thermal Properties of Polyvinyl Alcohol–Methylcellulose–Based Polymer Electrolytes. *Ionics (Kiel)* 26(12), 6083–6093 (2020). https://doi.org/10.1007/s11581-020-03753-9.
3. S. Alipoori, S. Mazinani, S.H. Aboutalebi, and F. Sharif, Review of PVA-Based Gel Polymer Electrolytes in Flexible Solid-State Supercapacitors: Opportunities and Challenges. *J Energy storage.* 27, 101072 (2020). https://doi.org/10.1016/j.est.2019.101072.
4. N. Almenara, R. Gueret, A.J. Huertas-Alonso, U.T. Veettil, M.H. Sipponen, and E. Lizundia, Lignin-Chitosan Gel Polymer Electrolytes for Stable Zn Electrodeposition. *ACS Sustain Chem Eng* 11(6), 2283–2294 (2023). https://doi.org/10.1021/acssuschemeng.2c05835.
5. B.K. Faris, A.A. Hassan, S.B. Aziz, M.A. Brza, A.M. Abdullah, A.A. Abdalrahman, O.A. Abu Ali, and D.I. Saleh, Impedance, Electrical Equivalent Circuit (Eec) Modeling, Structural (ftir and xrd), Dielectric, and Electric Modulus Study of mc-based Ion-Conducting Solid Polymer Electrolytes. *Materials* (2022). https://doi.org/10.3390/ma15010170.
6. S.N.M. Afini, N.A. Johari, H.H. Tajuddin, and S.K. Deraman, A Review: Ionic Conductivity of Solid Polymer Electrolyte Based Polyethylene Oxide. *Int. J. Electrochem. Sci.* 16(10), 211049 (2021). https://doi.org/10.20964/2021.10.53.
7. V. Bocharova, and A.P. Sokolov, Perspectives for Polymer Electrolytes: A View from Fundamentals of Ionic Conductivity. *Macromolecules* 53(11), 4141–4157 (2020). https://doi.org/10.1021/acs.macromol.9b02742.
8. N.F. Mazuki, A.F. Fuzlin, M.A. Saadiah, and A.S. Samsudin, An Investigation on the Abnormal Trend of the Conductivity Properties of CMC/PVA-Doped NH4Cl-Based Solid Biopolymer Electrolyte System. *Ionics (Kiel)* 25(6), 2657–2667 (2019). https://doi.org/10.1007/s11581-018-2734-9.
9. I.S. Noor, S.R. Majid, and A.K. Arof, Poly(vinyl alcohol)-LiBOB Complexes for Lithium-Air Cells. *Electrochim. Acta* 102, 149–160 (2013). https://doi.org/10.1016/j.electacta.2013.04.010.
10. M.F.Z. Kadir, and M.H. Hamsan, Green Electrolytes Based on Dextran-Chitosan Blend and the Effect of NH_4SCN as Proton Provider on the Electrical Response Studies. *Ionics (Kiel)* 24(8), 2379–2398 (2018). https://doi.org/10.1007/s11581-017-2380-7.
11. N.K. Zainuddin, and A.S. Samsudin, Investigation on the Effect of NH_4Br at Transport Properties in k–Carrageenan Based Biopolymer Electrolytes via Structural and Electrical Analysis. *Mater Today Commun* (2018). https://doi.org/10.1016/j.mtcomm.2018.01.004.
12. L. Li, C. Guan, A. Zhang, D. Chen, and Z. Qing, Thermal Stabilities and the Thermal Degradation Kinetics of Polyimides. *Polym. Degrad. Stab.* 84(3), 369–373 (2004). https://doi.org/10.1016/j.polymdegradstab.2003.11.007.
13. A.S. Samsudin, H.M. Lai, and M.I.N. Isa, Biopolymer Materials Based Carboxymethyl Cellulose as a Proton Conducting Biopolymer Electrolyte for Application in Rechargeable Proton Battery. *Electrochim. Acta* 129, 1–13 (2014). https://doi.org/10.1016/j.electacta.2014.02.074.
14. A. Jagadeesan, M. Sasikumar, R. Jeevani, H.A. Therese, N. Ananth, and P. Sivakumar, Fabrication of $BaTiO_3$ Ceramic Filler Incorporated PVC-PEMA Based Blend Nanocomposite Gel Polymer Electrolytes for Li Ion Battery Applications. *J. Mater. Sci. Mater. Electron.* 30(18), 17181–17194 (2019). https://doi.org/10.1007/s10854-019-02065-7.
15. S.K.S. Basha, G.S. Sundari, K.V. Kumar, and M.C. Rao, Preparation and Dielectric Properties of PVP-Based Polymer Electrolyte Films for Solid-State Battery Application. *Polym. Bull.* 75(3), 925–945 (2018). https://doi.org/10.1007/s00289-017-2072-5.
16. S. Karthikeyan, S. Selvasekarapandian, M. Premalatha, S. Monisha, G. Boopathi, G. Aristatil, A. Arun, and S. Madeswaran, Proton-Conducting I-Carrageenan-Based Biopolymer Electrolyte for Fuel Cell Application. *Ionics (Kiel)* 23(10), 2775–2780 (2017). https://doi.org/10.1007/s11581-016-1901-0.
17. M.N. Hafiza, and M.I.N. Isa, Solid Polymer Electrolyte Production from 2-Hydroxyethyl Cellulose: Effect of Ammonium Nitrate Composition on its Structural Properties. *Carbohydr. Polym.* (2017). https://doi.org/10.1016/j.carbpol.2017.02.033.

18. L.S. Kumar, P.C. Selvin, S. Selvasekarapandian, R. Manjuladevi, S. Monisha, and P. Perumal, Tamarind Seed Polysaccharide Biopolymer Membrane for Lithium-Ion Conducting Battery. *Ionics (Kiel)* 24(12), 3793–3803 (2018). https://doi.org/10.1007/s11581-018-2541-3.
19. M.F.Z. Kadir, S.R. Majid, and A.K. AROF, Plasticized Chitosan-PVA Blend Polymer Electrolyte Based Proton Battery. *Electrochim. Acta* 55(4), 1475–1482 (2010). https://doi.org/10.1016/j.electacta.2009.05.011.
20. S. Monisha, T. Mathavan, S. Selvasekarapandian, A.M.F. Benial, and M.P. Latha, Preparation and Characterization of Cellulose Acetate and Lithium Nitrate For Advanced Electrochemical Devices. *Ionics (Kiel)* 23(10), 2697–2706 (2017). https://doi.org/10.1007/s11581-016-1886-8.
21. M.F. Shukur, R. Ithnin, H.A. Illias, and M.F.Z. Kadir, Proton Conducting Polymer Electrolyte Based on Plasticized Chitosan-PEO Blend and Application in Electrochemical Devices. *In Opt Mater* 35(10), 1834–1841 (2013). https://doi.org/10.1016/j.optmat.2013.03.004.
22. A.K. Arof, M.F.Z. Kadir, R. Yahya, and Z. Aspanut, Chitosan-PEO Proton Conducting Polymer Electrolyte Membrane Doped with NH_4NO_3. *Mater. Res. Innov.* (2011). https://doi.org/10.1179/143307511X13031890748812.
23. N. M. Ghazali, N. F. Mazuki, and A. S. Samsudin, Characterization of biopolymer blend-based on alginate and poly (vinyl Alcohol) as an application for polymer host in polymer electrolyte, *IOP Conf Ser Mater Sci Eng*, vol. 1092, no. 1, 2021, https://doi.org/10.1088/1757-899x/1092/1/012047.
24. S. Hegde, V. Ravindrachary, S.D. Praveena, B.G. Ismayil, and R.N. Sagar, Microstructural, Dielectric, and Transport Properties of Proton-Conducting Solid Polymer Electrolyte for Battery Applications. *Ionics (Kiel)* 26(5), 2379–2394 (2020). https://doi.org/10.1007/s11581-019-03383-w.
25. Y. Shao and C. Zhang, 2023 Bruce-Vincent transference numbers from molecular dynamics simulations. *Journal of Chemical Physics*. https://doi.org/10.1063/5.0146608.
26. N.F. Mazuki, M.Z. Kufian, Y. Nagao, and A.S. Samsudin, Correlation studies between structural and ionic transport properties of lithium-ion hybrid gel polymer electrolytes based PMMA-PLA. *J. Polym. Environ.* 30(5), 1864–1879 (2022). https://doi.org/10.1007/s10924-021-02317-w
27. N.K. Zainuddin, N.M.J. Rasali, N.F. Mazuki, M.A. Saadiah, and A.S. Samsudin, Investigation on favourable ionic conduction based on CMC-K carrageenan proton conducting hybrid solid biopolymer electrolytes for applications in EDLC. *Int. J. Hydrogen Energy* 45(15), 8727–8741 (2020). https://doi.org/10.1016/j.ijhydene.2020.01.038
28. M.N. Hafiza, and M.I.N. Isa, Ionic conductivity and conduction mechanism studies of CMC/Chitosan biopolymer blend electrolytes. *Res. J. Recent Sci* 3(11), 50–56 (2014).
29. M.A. Saadiah, Y. Nagao, and A.S. Samsudin, Proton (H+) transport properties of CMC–PVA blended polymer solid electrolyte doped with NH_4NO_3. *Int. J. Hydrogen Energy* 45(29), 14880–14896 (2020). https://doi.org/10.1016/j.ijhydene.2020.03.213
30. S. Ramesh, C.W. Liew, and K. Ramesh, Evaluation and investigation on the effect of ionic liquid onto PMMA-PVC gel polymer blend electrolytes. *J. Non. Cryst. Solids* 357(10), 2132–2138 (2011). https://doi.org/10.1016/j.jnoncrysol.2011.03.004
31. A.K. Arof, S. Amirudin, S.Z. Yusof, and I.M. Noor, A method based on impedance spectroscopy to determine transport properties of polymer electrolytes. *Phys. Chem. Chem. Phys.* 16(5) (2014). https://doi.org/10.1039/c3cp53830c
32. A.M. Abdullah, S.B. Aziz, and S.R. Saeed, Structural and electrical properties of polyvinyl alcohol (PVA): Methyl cellulose (MC) based solid polymer blend electrolytes inserted with sodium iodide (NaI) salt. *Arab. J. Chem.* 14(11), 103388 (2021). https://doi.org/10.1016/j.arabjc.2021.103388
33. A.A. Abdalrahman, S.B. Aziz, and W.O. Karim, EIS and FTIR approaches to study the ion transport parameters and relaxation dynamics of Na^{+1} ion in SPE based on MC polymer inserted with sodium salt. *Results Phys.* 36, 105439 (2022). https://doi.org/10.1016/j.rinp.2022.105439
34. A.A. Chen, and R.V. Pappu, Quantitative Characterization of Ion Pairing and Cluster Formation in Strong 1:1 Electrolytes. *J. Phys. Chem. B* 111(23), 6469–6478 (2007). https://doi.org/10.1021/jp0708547.
35. M.N. Hafiza, and M.I. Isa, Ionic Conductivity and Conduction Mechanism Studies of CMC/ Chitosan Biopolymer Blend Electrolytes. *Res J Recent Sci* 3(11), 2502 (2014).
36. M.A. Saadiah, Y. Nagao, and A.S. Samsudin, Proton (H+) Transport Properties of CMC–PVA Blended Polymer Solid Electrolyte Doped with NH_4NO_3. *Int. J. Hydrogen Energy* 45(29), 14880–14896 (2020). https://doi.org/10.1016/j.ijhydene.2020.03.213.
37. S. Ramesh, C.W. Liew, and K. Ramesh, Evaluation and Investigation on the Effect of Ionic Liquid Onto PMMA-PVC Gel Polymer Blend Electrolytes. *J. Non Cryst. Solids* 357(10), 2132–2138 (2011). https://doi.org/10.1016/j.jnoncrysol.2011.03.004.
38. L.D. McIntosh, M.W. Schulze, M.T. Irwin, M.A. Hillmyer, and T.P. Lodge, Evolution of Morphology, Modulus, and Conductivity in Polymer Electrolytes Prepared via Polymerization-Induced Phase Separation. *Macromolecules* 48(5), 1418–1428 (2015). https://doi.org/10.1021/ma502281k.
39. M.W. Schulze, L.D. McIntosh, M.A. Hillmyer, and T.P. Lodge, High-Modulus, High-Conductivity Nanostructured Polymer Electrolyte Membranes via Polymerization-Induced Phase Separation. *Nano Lett.* 14(1), 122–126 (2014). https://doi.org/10.1021/nl4034818.
40. J. Wang et al., The Synergistic Effects of Dual Substitution of Bi and Ce on Ionic Conductivity of Li7La3Zr2O12 Solid Electrolyte. *Ceram. Int.* 50(4), 6472–6480 (2024). https://doi.org/10.1016/j.ceramint.2023.11.391.
41. P.G. Bruce, and C.A. Vincent, Steady State Current Flow in Solid Binary Electrolyte Cells. *J. Electroanal. Chem.* 225(1–2), 1–17 (1987). https://doi.org/10.1016/0022-0728(87)80001-3.
42. N.A.M. Noor, and M.I.N. Isa, Investigation on Transport and Thermal Studies of Solid Polymer Electrolyte Based on Carboxymethyl Cellulose Doped Ammonium Thiocyanate for Potential Application in Electrochemical Devices. *Int. J. Hydrogen Energy* (2019). https://doi.org/10.1016/j.ijhydene.2019.02.062.